Thermal and fluid flow simulation of a compact heat exchanger with micropillar

Edemar Morsch Filho[1], Ariany Pereira Moreira [2], Elaine Maria Cardoso[1]

[1]*Dept. of Aeronautical Engineering, São Paulo State University*
Av. Profa. Isette Corrêa Fontão, 505 - Jardim das Flores, São João da Boa Vista - SP, 13876-750, Brazil
edemar.filho@unesp.br, elaine.cardoso@unesp.br
[2]*School of Engineering, São Paulo State University*
Av. Brasil Sul, 56 - Centro, Ilha Solteira - SP, 15385-000, Brazil
ariany.moreira@unesp.br

Abstract. Technological advances in manufacturing processes and materials have enabled the miniaturization of electronic components, which is positive in many ways but also introduces thermal management challenges due to the increased power density of components and reduced surface area for heat dissipation. In this sense, the use of compact heat exchangers presents itself as a possibility for controlling the temperature of these devices, such as those based on micropillars and microchannels. This study is based on the numerical simulation of a compact heat exchanger of square micropillars with 0.35 mm, with different arrangement configurations. Deionized water is used as the working fluid for the single-phase flow regime under different mass velocities (335-1414 kg/m²s) and input heat powers ($\sim$ 15 W). The modeling was implemented in the Ansys Fluent software, and the results obtained were validated and compared with experimental data, where data adherence was verified. Moreover, the numerical results were compared with another reference case based on a plain surface without micropillars. In terms of pressure drop and micropillar temperature, discrepancies are more pronounced for the plain case (overestimation), but the simulations capture the overall temperature and pressure trends of all the cases. The results show that micro-pin fin heat sinks can be very effective as a thermal management technique.

Keywords: Micro-pin fins, Heat sink, Micropillars, Thermal performance index, Thermal management

1 Introduction

Optimized heat sinks are helpful in solving thermal and fluid dynamic problems encountered at the microscale. McHale and Garimella [1] investigated trapezoidal microchannels with different aspect ratios to improve heat transfer. The authors observed that both the aspect ratio and the sidewall angle of the trapezoidal channel increase heat transfer. Thus, it is suggested that adjusting geometric parameters can be an effective strategy to optimize the thermal performance of devices that use microchannels, such as compact heat exchangers and electronic cooling systems. Micropillars, another example of optimized structures, are promising for improving heat transfer in convective boiling [2, 3]. For example, Prajapati et al. [4] carried out a comparative experimental study of micropillars with parallel microchannels. The results showed a higher heat transfer coefficient for the micropillar-based heatsink, with a negligible penalty in pressure drop. In general, such studies show that the presence of micropillars in the flow leads to the constant formation of the hydrodynamic and thermal boundary layers at the edges of each fin, effectively reducing the thickness of the boundary layer [5].

The study of compact heat exchangers encompasses a range of topics, including the selection of appropriate fluids, geometry optimization, and advancements in 3D printing technologies. In the study of Kempers et al. [6], a high-performance water-cooled micro heat sink for the thermal management of high heat flux microelectronics was fabricated using an additive manufacturing process to produce complex flow, which is impossible to fabricate with traditional processes. A prototype heat sink was fabricated and tested at heat fluxes exceeding 1000 W/cm^2. Inlet water at 20 °C corresponded to a measured base temperature of 54 °C at an applied heat flux of 1000 W/cm^2. The work of Shen et al. [7] investigates using impingement jet nested arrays to strengthen the thermal performance of double-layer microchannel heat sinks based on 3D printing technologies. The thermal control was very effective, with a reduction in peak temperature of more than 20 K lower than traditional microchannel heat sinks. Even though the proposed structure yields a higher pressure drop penalty, the overall thermal performance

factor that balances the influence of heat transfer augmentation and pressure drop penalty still favors the proposed geometry. The study of Zhang et al. [8] developed a water-cooled pseudo 3D heat sink structure using a two-layer heat sink model, and the authors performed a topology optimization. Compared with the one-layer heat sink model, the two-layer heat sink model was proved to have better heat transfer capability. Gilmore et al. [9] studied manifold microchannel heat sink structures for high heat flux cooling by applying topology optimization within a multi-objective 3D conjugate heat transfer model. Compared to rectangular manifold microchannels, the proposed structures reduce pressure drop by 17% by suppressing stagnation regions and a more substantial 79.2% by limiting nozzle constrictions. This structure simultaneously reduces thermal resistance by 22.4% by introducing pins and constrictions, which augment jet impingement and counteract streamwise heating of the fluid.

The above scenario suggests that compact heat exchangers can address the industry's typical thermal challenges. Therefore, this work aims to study heat transfer and pressure drop of water through a heat exchanger with square micropillars, with different arrangements (aligned and staggered), in addition to a reference surface — flat, without micropillars — and validate them with experimental data.

2 Methodology

The numerical problem described in this work is inspired by an experiment conducted at NEST-n (Nano and Microscale Heat Transfer Lab) [10]. The experimental setup consisted of a QUIMIS® Q241M thermostatic bath to control the water flow and its inlet temperature into the preheater. A Swagelok® needle valve was used for fine flow adjustment, and a Yokogawa Coriolis mass flow meter (RCEP25S, 0.10% uncertainty) measured the flow rate. The preheater consisted of a coiled electric resistance around a copper pipe (diameter of 9.5 mm, 800 mm long), insulated with polyurethane foam and PVC. Absolute pressure transducers (PXM309 OmegaTM, $\pm$ 0.25% FS) and K-type thermocouples measured the pressure and temperature at the inlet and outlet of the test section. The heat sink was made of a copper block with machined square micropillars. K-type thermocouples at the heat sink's base measured the temperature to determine the heat flux. A 250 W/220 V cartridge heater powered by a TECTROL power supply provided the necessary heat for the tests. A polycarbonate plate provided thermal insulation and flow visualization, while a ceramic mold insulated the walls.

Considering the numerical modeling of this experimental setup, the overall geometry of the problem is illustrated in Fig. 1. The fluid domain represents the water flow, represented by the brown color, while the solid part, made of copper, is blue. The remaining walls are not simulated; their influence is added through boundary conditions (adiabatic and non-slip). Water flows from the inlet to the outlet, and the heat is added to the geometry's central bottom part.

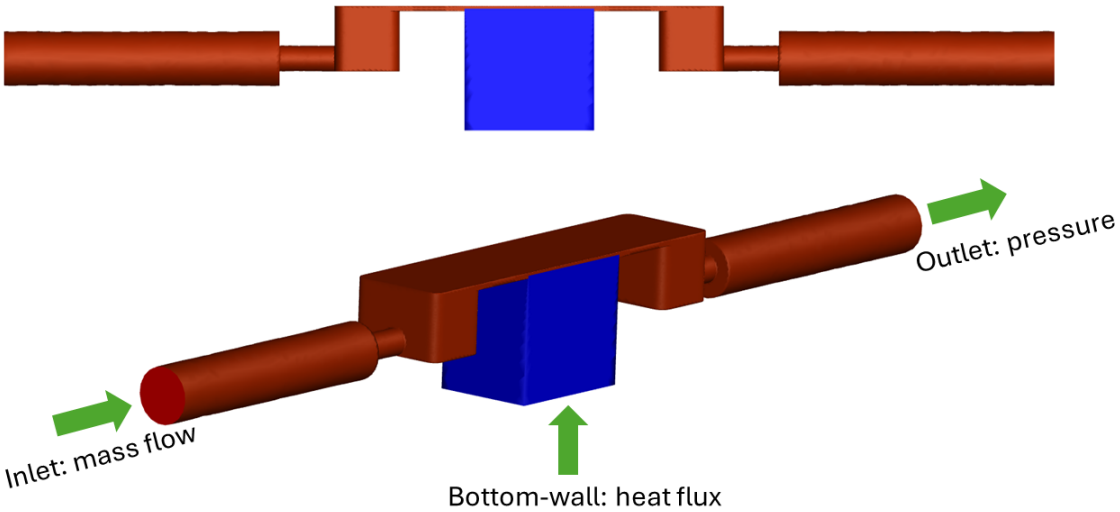

Figure 1. Numerical domain

This main configuration will be tested for two different arrangement configurations: aligned and staggered. A view of each of these configurations is given in Fig.2. The micropillars are cubes with 0,35×0,35×0,35 mm. For the aligned configuration, the distances are $S_L = S_T = 0,55$ mm, while for the staggered $S_L = S_T = 0,80$

mm.

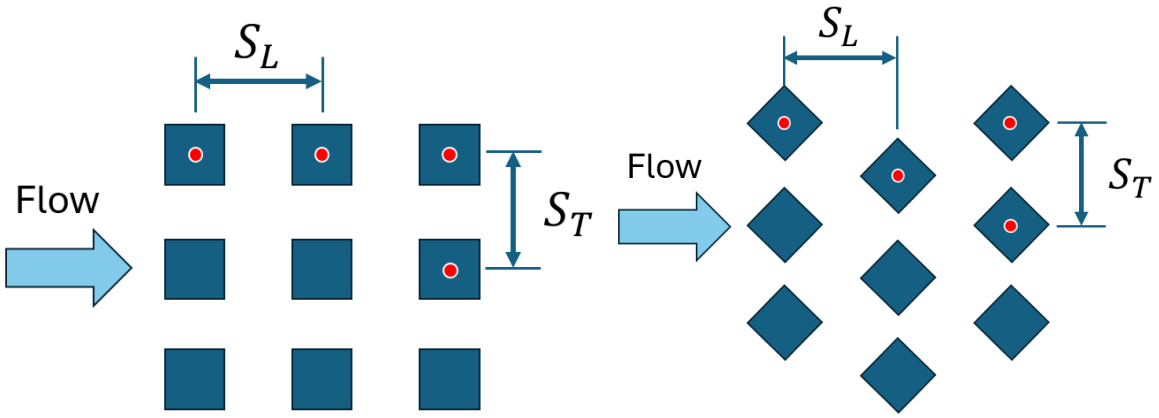

(a) Aligned (b) Staggered

Figure 2. Micropillar arrangements

A third case without any micropillars (plain case) is also assessed. This benchmark case will be used to determine the improvement in the thermal and hydraulic performance of the heat exchanger.

2.1 Mesh

Three meshes are generated to perform a convergence and grid independence test. For all meshes, a refinement was applied for regions with corners and the fluid domain around the micropillars. Also, boundary layers were added at the fluid domain near the wall. The pressure drop between the inlet and outlet (ΔP) and the average micropillar temperature (T_p) were monitored for each mesh. The main results are summarized in Tab.1.

Table 1. Grid independence test

	Plain			Aligned			Staggered		
Mesh	Cells	ΔP [kPa]	T_p [°C]	Cells	ΔP [kPa]	T_p [°C]	Cells	ΔP [kPa]	T_p [°C]
1	51,242	2.331	27.01	70,642	5.418	24.117	73,645	7.130	26.96
2	90,134	2.786	27.51	120,966	5.998	24.712	131,431	7.491	27.17
3	241,346	2.805	27.57	272,494	6.058	24.767	286,731	7.502	27.23

Based on the above results, Mesh 3 was selected as its computational cost was affordable. Its minimum, maximum and averaged orthogonal quality are 0.15, 0.997, and 0.779, respectively. Its maximum aspect ratio is 64. These parameters are obtained using polyhedra cells.

2.2 Governing equations

To solve the flow and the heat transfer related to this study, the continuity (eq. 1), momentum (eq. 2), and energy (eq. 3) equations are solved, considering an incompressible flow, Newtonian fluid, steady-state condition, without body forces, viscous work, and internal energy sources.

Continuity:

$$\nabla \cdot \vec{V} = 0 \tag{1}$$

Momentum:

$$\rho(\vec{V} \cdot \nabla)\vec{V} = -\nabla p + \mu \nabla^2 \vec{V} \tag{2}$$

Energy:

$$\vec{V} \cdot \nabla T = \alpha \nabla^2 T \tag{3}$$

2.3 Boundary conditions

The boundary conditions used in this work are based on experimental results, where the mass flow, the heating power, and the inlet temperature were controlled. Therefore, at the inlet, the boundary conditions for the mass flow (kg/s) and temperature (°C) are prescribed, while at the outlet, the manometric pressure was set as 0 Pa. For the interface between the fluid domain and solid domain, a no-slip condition ($\vec{V} = 0$) was prescribed, in addition to the continuity of temperature ($T_f = T_s$) and heat flux conservation ($-k_f \partial T_f \partial n = -k_s \frac{\partial T_s}{\partial n}$). The subscripts f and s are valid for fluid and solid domains, respectively. For simplification, the external walls of the domain are adiabatic, except for the copper's base, where a heat flux was prescribed.

The mass flow of the simulation is small, with Reynolds number (based on the hydraulic diameter) not greater than 675. Therefore it is assumed that there will be a laminar flow for all the cases.

2.4 Study cases

The simulations are performed according to the parameters of Tab. 2, where G is the mass-velocity flux (based on the minimum area of the test section), T_{in} is the inlet temperature of the water, and Q is the power applied at the bottom wall of the copper.

Table 2. Study cases

Arrangement	G [kg/m^{2}s]	T_{in} [°C]	Q [W]
Plain	335.25	24.60	15.43
Plain	498.06	24.35	15.43
Plain	634.82	23.50	15.43
Plain	723.98	23.10	15.42
Plain	802.57	22.94	15.46
Plain	848.71	22.82	15.48
Plain	890.42	22.59	15.49
Plain	985.17	22.56	15.50
Plain	1046.92	22.61	15.50
Plain	1140.34	22.68	15.50
Plain	1240.41	22.90	15.50
Aligned	458.69	22.30	16.14
Aligned	571.31	22.31	16.23
Aligned	648.25	22.38	16.37
Aligned	737.61	22.38	16.47
Aligned	847.52	22.41	16.42
Aligned	994.09	22.48	16.59
Aligned	1055.46	22.45	16.63
Aligned	1134.02	22.48	16.66
Staggered	382.66	26.46	15.96
Staggered	550.54	26.36	15.98
Staggered	748.48	25.02	15.79
Staggered	820.72	23.79	15.74
Staggered	934.06	23.40	15.74
Staggered	1121.73	22.96	15.83
Staggered	1295.92	23.45	15.87
Staggered	1414.03	23.50	15.83

2.5 Numerical schemes and convergence criteria

A coupled scheme with second-order for pressure, momentum, and energy, with relaxation factors of 0.5, 0.5, and 0.75, respectively, is used for pressure-velocity evaluation. For convergence criteria, residuals lower than 1×10^{-5} for all the conservation equations, except for the energy, where a residual of 1×10^{-9} is assumed. These simulations are performed using the software Ansys Fluent 2022 R2, with the license provided by Unesp.

3 Results

This section presents, discusses, and compares the numerical results with experimental data. The numerical results are presented, discussed, compared with experimental data in this section. Figure 3 summarizes the pressure drop achieved through the heat exchanger, measured between the inlet and outlet, for different mass flux velocities and arrangements. As expected, the plain configuration without micropillars presents the lowest pressure drop across the test section, while the aligned arrangement shows a smaller pressure drop than the staggered case when the experimental data are assessed. This behavior can be attributed to the more complex flow pattern for the staggered arrangement configuration, as the flow can be divided and redirected, creating vortices, greater disturbance, and separation of the flow, causing an increase in pressure drop. In the aligned arrangement the fluid flows preferentially along the primary channels, parallel to the main flow direction. Similar observations were made by Reeser et al. [11], who reported a 50% increase in pressure drop for the staggered arrangement configuration compared to the aligned arrangement. However, the results are very close for identical mass-velocity fluxes when looking at the numerical data between the aligned and staggered cases.

Except for the staggered configuration, the numerical solution was overestimated compared to experimental data; however, it still presents a similar tendency of pressure drop augmentation with mass-velocity flux. Although there is no conclusive answer to this question, one possible reason for such a discrepancy can be attributed to uncertainty about the test-section height, ideally 0,35 mm. Variations in the microscopic dimensions across the experimental test section can influence the flow pressure. Additionally, surface imperfections — such as slight irregularities or sharp edges between the channels resulting from the manufacturing process— may also contribute to these discrepancies, as the numerical simulation assumes a perfectly smooth surface.

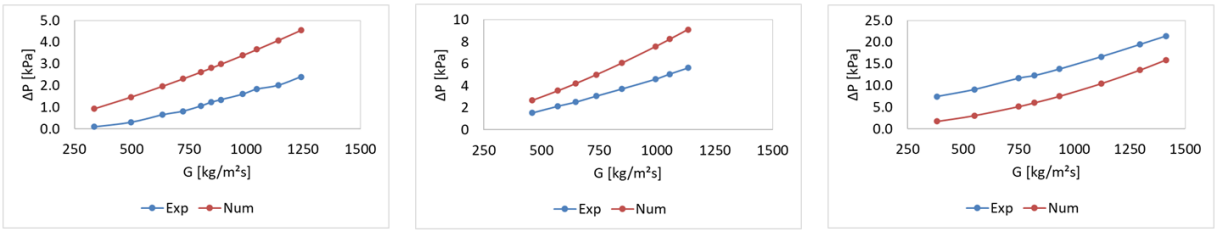

(a) Plain (b) Aligned (c) Staggered

Figure 3. Pressure drop

Figure 4 shows the flow's outlet temperature (T_{out}), measured after the test section. Since the heat input was very similar among the cases, the outlet temperature drops with the mass velocity of the flow. The highest levels are obtained for the staggered configuration, followed by the aligned and the plain, respectively. The plain configuration shows temperatures at the outlet lower than the plain case, which can be explained by the fact that in the plain geometry, the heat available is not efficiently transferred to the fluid due to the lack of pillars. The presence of pillars increases the area for heat transfer and promotes some mixture of the fluid, both conditions that promote the outlet's temperature increase. The percentage difference between the numerical and experimental results is below 3% for the plain and aligned cases, whereas it rises to 12% for the staggered geometry. For the staggered configuration, this difference reduces at greater mass velocities, while it increases for the aligned case and remains almost constant for the plain.

Figure 5 summarizes the micropillar temperature (T_p) of each case. As expected, this temperature reduces when the mass velocity increases. It is interesting to notice that the numerical simulation captures the overall behavior, but there is more discrepancy between the results for the plain cases. One possibility for this may be related to the procedure of obtaining these data. The wall temperature is obtained in the experimental analysis by linear extrapolating three measured temperatures from the thermocouples embedded in the copper block. In contrast, in the numerical evaluation, it is an average of the entire upper surface of the copper in contact with the flow.

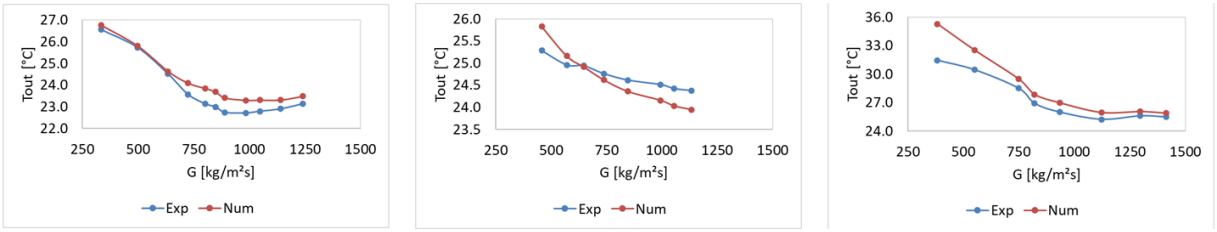

(a) Plain (b) Aligned (c) Staggered

Figure 4. Outlet temperature

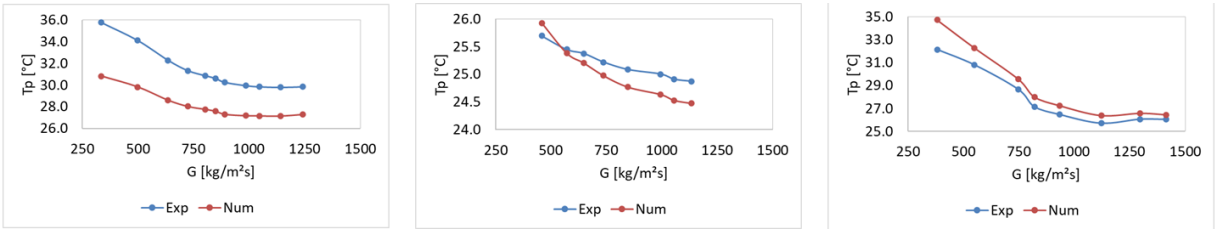

(a) Plain (b) Aligned (c) Staggered

Figure 5. Micropillar temperature

Finally, Fig. 6 compares the numerical data obtained for each geometry. The influence of micropillar, especially for the staggered configuration, is evident in these results, in both pressure and temperatures achieved by the fluid. Interestingly, the plain case can achieve the highest micropillar temperature (T_p) for a given mass-velocity flux; however, its poor mixing characteristics result in the lowest outlet temperatures (T_{out}). As mentioned previously, the pressure drop is similar for both cases with micropillars.

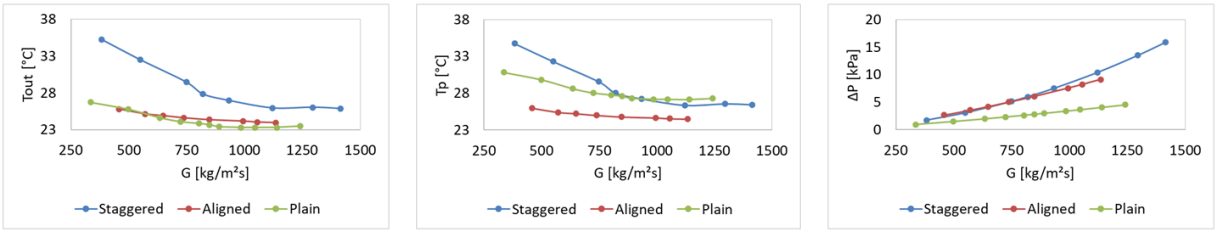

(a) Outlet temperature (b) Micropillar temperature (c) Pressure drop

Figure 6. Comparison of numerical configurations

4 Conclusions

The study presented a comprehensive numerical analysis of the heat transfer and fluid flow features in a heat exchanger with different micropillar arrangements. The numerical results showed that the staggered and aligned micropillar arrangements exhibited similar pressure drop, followed by the plain case, although this tendency for the micropillar cases is not observed in the experimental data. Except for the staggered case, the numerical simulations tended to overestimate the pressure drop compared to experimental data.

Regarding the temperature levels, the staggered arrangement resulted in the highest outlet temperature, indicating better heat transfer performance compared to the aligned and plain cases. The numerical simulations captured the overall temperature trends, although discrepancies were more pronounced in the plain case, likely due to differences in measurement techniques between the numerical and experimental methods.

Therefore, the staggered configuration, while causing a higher pressure drop, provides better heat transfer efficiency, and the numerical model captured this despite some overestimations. Future work should focus on refining the numerical model and exploring additional geometric configurations to improve results' performance and convergence.

Acknowledgements. E.M. Cardoso is grateful for the financial support from Conselho Nacional de Desenvolvimento Científico e Tecnológico (grants number 309848/2020-2 and 305040/2023-5) and Fundação de Amparo à Pesquisa do Estado de São Paulo (grants numbers 2013/15431-7, 2019/02566-8, 2022/15765-1 and 2023/03492-3).

Authorship statement. The authors hereby confirm that they are the solely liable persons responsible for the authorship of this work and that all material that has been herein included as part of the present paper is either the property (and authorship) of the authors or has the permission of the owners to be included here.

References

[1] J. P. McHale and S. V. Garimella. Heat transfer in trapezoidal microchannels of various aspect ratios. *International Journal of Heat and Mass Transfer*, vol. 53, n. 1, pp. 365–375, 2010.
[2] D. Deng, L. Zeng, and W. Sun. A review on flow boiling enhancement and fabrication of enhanced microchannels of microchannel heat sinks. *International Journal of Heat and Mass Transfer*, vol. 175, pp. 121332, 2021.
[3] N. K. Vidhyarthi, S. Deb, S. S. Gajghate, E. M. Cardoso, M. Das, S. Pal, and A. K. Das. Influence of microfin tube on heat transfer during flow boiling of r134a refrigerant. *Journal of Engineering*, vol. 2024, n. 1, pp. 6824128, 2024.
[4] Y. K. Prajapati, M. Pathak, and M. Kaleem Khan. A comparative study of flow boiling heat transfer in three different configurations of microchannels. *International Journal of Heat and Mass Transfer*, vol. 85, pp. 711–722, 2015.
[5] X. Ma, X. Ji, J. Wang, X. Yang, Y. Zhang, and J. Wei. Flow boiling instability and pressure drop characteristics based on micro-pin-finned surfaces in a microchannel heat sink. *International Journal of Heat and Mass Transfer*, vol. 195, pp. 123168, 2022.
[6] R. Kempers, J. Colenbrander, W. Tan, R. Chen, and A. Robinson. Experimental characterization of a hybrid impinging microjet-microchannel heat sink fabricated using high-volume metal additive manufacturing. *International Journal of Thermofluids*, vol. 5-6, pp. 100029, 2020.
[7] H. Shen, Z. Zhang, X. Ge, H. Liu, G. Xie, and C.-C. Wang. Thermal analysis and experimental verification on double-layer microchannel heat sinks with impact jet nested arrays. *International Journal of Heat and Mass Transfer*, vol. 209, pp. 124169, 2023.
[8] T. Zhang, Y. Fu, and X. Yang. A pseudo 3d cooling heat sink model designed by multi-objective topology optimization method. *Meccanica*, vol. 57, pp. 2101–2116, 2022.
[9] N. Gilmore, V. Timchenko, and C. Menictas. Manifold microchannel heat sink topology optimisation. *International Journal of Heat and Mass Transfer*, vol. 170, pp. 121025, 2021.
[10] J. M. Nunes, de J. D. Oliveira, J. B. Copetti, S. S. Gajghate, U. Banerjee, S. K. Mitra, and E. M. Cardoso. Thermal performance analysis of micro pin fin heat sinks under different flow conditions. *Energies*, vol. 16, n. 7, 2023.
[11] A. Reeser, A. Bar-Cohen, and G. Hetsroni. High quality flow boiling heat transfer and pressure drop in microgap pin fin arrays. *International Journal of Heat and Mass Transfer*, vol. 78, pp. 974–985, 2014.